Nanoscale

Accepted Manuscript

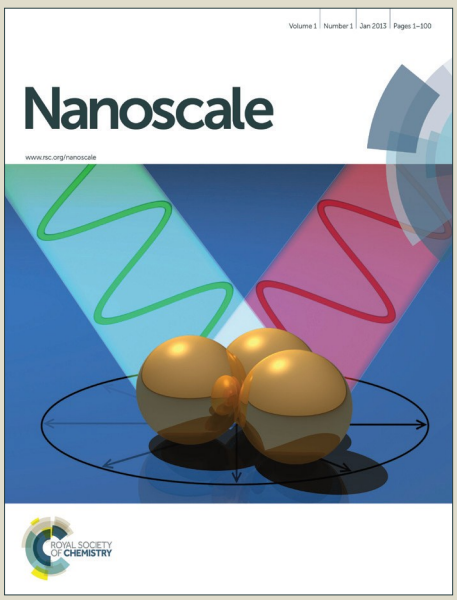

ROYAL SOCIETY OF CHEMISTRY

www.rsc.org/nanoscale

Nanoscale

COMMUNICATION

Received 00th January 20xx,
Accepted 00th January 20xx

DOI: 10.1039/x0xx00000x

www.rsc.org/

Solubility Studies of Inorganic-Organic Hybrid Nanoparticle Photoresists with Different Surface Functional Groups

Li Li*, Souvik Chakrabarty, Jing Jiang, Ben Zhang, Christopher Ober, Emmanuel P. Giannelis*

The solubility behavior of Hf and Zr based hybrid nanoparticles with different surface ligands in different concentrations of photoacid generator as potential EUV photoresists was investigated in detail. The nanoparticles regardless of core or ligand chemistry have a hydrodynamic diameter of 2-3 nm and a very narrow size distribution in organic solvents. The Hansen solubility parameters for nanoparticles functionalized with IBA and 2MBA have the highest contributions from the dispersion interaction than those with tDMA and MAA, which show more polar character. The nanoparticles functionalized with unsaturated surface ligands showed more apparent solubility changes after exposure to DUV than those with saturated. The solubility differences after exposure are more pronounced for films containing a higher amount of photoacid generator. The work reported here provides materials selection criteria and processing strategies for the design of high performance EUV photoresists.

Urgent demands in microelectronics and advanced device nanofabrication require the development of next generation lithography technologies that can provide the necessary high-resolution patterning. Extreme ultraviolet (EUV) lithography is expected to provide practical solutions for sub-10 nm, industry-scale fabrication because of its advantages including high resolution patterning, easy processing, high-throughput and fewer design restrictions.[1-3] The next generation EUV photoresists are required to have appropriate physicochemical properties for high resolution and small scale patterning, such as high etch resistance, high imaging quality and appropriate UV light absorption. Hybrid organic-inorganic hybrid photoresists are considered potential candidates for industry scale sub-16 nm photo-patterning because of their advantages in etch resistant, processing simplicity and chemical/thermal stability.[4-8] One requirement is that the size of the nanoparticles used needs to be small to avoid excessive Rayleigh scattering.[9] In addition, small particle size with narrow size distribution are also of great significance for decreasing the length edge roughness (LER)/contact edge roughness (CER) and obtaining high resolution patterning.[1]

a. *Department of Materials Science and Engineering, Cornell University, Ithaca, NY, 14853, USA. Email: lilicmu@gmail.com; Email: epg2@cornell.edu Tel: +1-607-255-6980. FAX: + 1-607-255-2365; Electronic Supplementary Information (ESI) available: See DOI: 10.1039/x0xx00000x*

TiO_2 has been used previously in nanoimprint lithography for large scale patterning using a polymerizable liquid titanium methacrylate mixture.[8] Application of TiO_2 patterning was extended to step-and-flash imprint lithography from acrylate based formulations.[7] Stowers et al. used hafinium and zirconium oxide sulfates for 15-nm and 36-nm line patterning by e-beam lithography, with 25% w/w tetramethylammonium hydroxide as the developer.[10] Our group has pioneered hybrid double-tone EUV photoresists based on ZrO_2 and HfO_2 nanoparticles, which allows both positive and negative tones to be formed in the same material with different solutions as the developer.[4, 11] The ZrO_2 based photoresists have shown high sensitivity in patterning 26 nm and 32 nm lines with a dose of 4.2 and 5.6 mJ/cm^2, respectively, indicating their excellent potential for next generation photoresists with high resolution patterning. An initial discussion about particle size changes upon UV exposure and the associated patterning mechanism has been included in an earlier publication.[12]

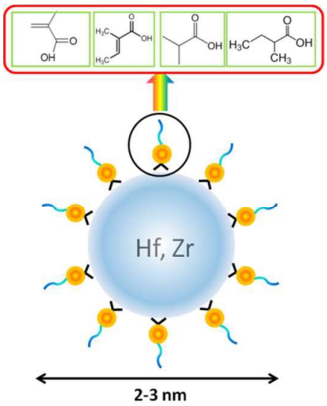

Schematic 1. Hybrid nanoparticles composed of a metal oxide core (HfO_2 or ZrO_2) and carboxylic acid ligands as surface functionalization groups. The ligands from left to right are: methacrylic acid (MMA), trans-2,3 dimethyl acrylic acid (TDMA), isobutyric acid (IBA), and 2-methylbutanoic acid (2MBA).

Dispersion/solubility of the nanoparticles in a solvent is crucial for the development of high performance hybrid photoresists.[5] Surface ligands can stabilize the nanoparticles in the solvent and prevent physical or chemical aggregation of the nanoparticles. The solubility parameters, which were widely used to assess the physical properties of polymers,[13, 14] can also be used to evaluate

the affinity between solvent molecules and nanoparticles. Studying the dispersion and solubility characteristics of the hybrid nanoparticles in organic solvents is important for understanding their physicochemical properties and providing strategies for the design of functionalized hybrid materials as high performance EUV photoresists.

In this paper, HfO_2 and ZrO_2 nanoparticles surface-modified with different ligands are prepared, as shown in schematic 1, and their detailed relationship between their surface chemistry and solubility in different solvents is established. The results show that nanoparticles surface-modified with unsaturated ligands have a higher solubility change after UV exposure than those with saturated ligands. The detailed physicochemical characterization provides a systematic framework to understand the patterning mechanism of our novel inorganic/organic nanoparticles as EUV resists and offers strategies for optimizing their performance as next-generation photoresists.

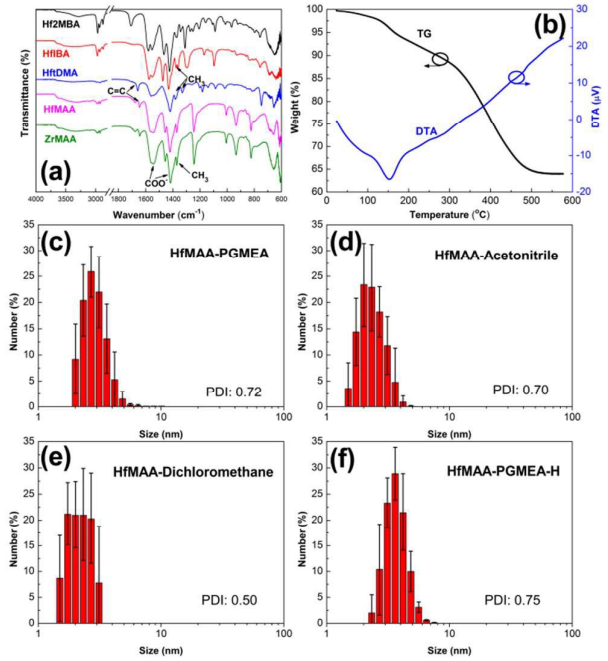

Figure 1. (a) FTIR spectra of hybrid nanoparticles with different surface chemistries and metal oxide cores; (b) thermal analysis of HfIBA hybrid nanoparticle; size distribution and hydrodynamic radius obtained by dynamic light scattering of HfMAA nanoparticles in low concentration (10mg of nanoparticles in 5mL solvent) dispersed in (c) PGMEA, (d) acetonitrile, (e) dichloromethane at low concentration and (f) in high concentration (10mg in 250 mg suspension).

The detailed experimental setup for measuring solubility and materials synthesis/characterization is provided in the supplementary information. The hybrid nanoparticles with different surface chemistry were synthesized by the sol-gel method as described previously.[12] FTIR spectra of HfO_2 and ZrO_2 based nanoparticles are shown in Figure 1-a. The peaks in the spectrum are consistent with the characteristic groups of the corresponding surface ligands. All nanoparticle systems show peaks at ~1420 and 1540 cm^{-1}, which are related to the symmetric and asymmetric stretching bands, respectively, of COO^- confirming the binding of the carboxylic groups to the nanoparticles.[15-17] The strong signals at 1640 cm^{-1} for HfMAA and ZrMAA as well as 1660 cm^{-1} for HftDMA originate from the stretching bands of C=C double bonds. On the other hand, no peaks are observed within the characteristic range of C=C double bonds (1620 cm^{-1} and 1680 cm^{-1}) for HfIBA and Hf2MBA. This result is consistent with the unsaturated nature of MAA and tDMA. The IR spectrum of ZrMAA is similar to that of HfMAA. In addition, the spectra of other ZrO_2 based nanoparticles (not shown here) also show similar peaks to those of HfO_2 nanoparticles suggesting that the nature of the core is not critical to the ligand bonding. Thermal analysis of HfIBA hybrid nanoparticles is shown in Figure 1-b. Two primary weight losses are observed in the range of 150 ºC to 300 ºC and again from 300 ºC to 500 ºC with a loss of 5 wt% and 25 wt%, respectively. The weight loss at ~150 ºC is attributed to evaporation of any loosely adsorbed water or ligands.[5, 18] Between 300 ºC to 500ºC, the weight loss is due to dexydroxylation and decomposition of the ligands leaving behind the inorganic core. The results from the thermal analysis for all hybrid nanoparticles are summarized in Table S1. The inorganic content in both HfO_2 and ZrO_2 systems varies with the type of ligands but it is approximately between 50 and 65 wt%.

To evaluate the dispersion of the nanoparticles in different solvents (PGEMA, acetonitrile, and dichloromethane), their sizes were measured by light scattering. The nanoparticles disperse well in all solvents with an apparent size of 2-3 nm. Figure 1-f shows the dispersion of HfMAA in PGMEA at a concentration typically used in photolithography evaluation (25 mg in 250 mg suspension). The sizes of the nanoparticles remained virtually unchanged (3-4 nm) with a narrow size distribution, indicating an excellent dispersion capability even at higher concentrations (results not shown). The particle size of all Zr-based nanoparticles dissolved in PGEMA, reported as one of the primary solvents used for lithography,[19] was also measured. Similar to HfMAA, all nanoparticles show a hydrodynamic diameter of 2-3 nm with a narrow size distribution.

As we reported previously, the nanoparticles are patternable under DUV, 193nm, e-beam and EUV lithography with addition of appropriate amounts of photoacid generator (PAG) and developer.[4] SEM images of nanoscale patterns after DUV exposure are shown in Figure S1. Sharp negative tone patterning lines, with the line width and spacing marked on the images, can be seen. No apparent difference was observed in patterning from Hf- and Zr-nanoparticles.

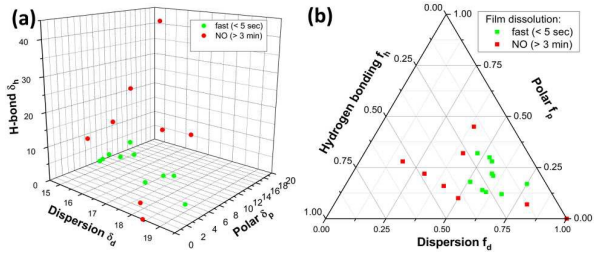

Figure 2. (a) Three dimensional plot of Hansen solubility parameters for HfIBA films in 17 different solvents; and (b) Triangular teas graph of the HfIBA film in the different solvents. Different colors refer to different solubility of the film in the corresponding solvent: red refers to films that are insoluble within 3 minutes; green refers to films soluble within 5 seconds.

To gain a better understanding of the mechanism of photoresist development, the solubility of the nanoparticles in different solvents was evaluated in detail using the concept of solubility parameters. The compatibility between the solvent and the solute can be predicted using the cohesive energy density.[20] The solubility parameter δ is defined as:[21]

$$\delta = (c)^{1/2} = (\frac{E}{V})^{1/2} \quad (1)$$

where, c is the energy density of the liquid, E is the vaporization energy, and V is the molar volume of the solvent. The Hansen solubility parameter is considered one of the most widely used parameters for evaluation of the affinity between polymers and solvents.[22] The Hansen solubility parameter is divided into three components: δ_d, δ_p, and δ_h, representing the respective contributions from nonpolar atomic dispersion interactions, polar molecular interactions, and hydrogen bonding molecular interactions to the cohesive energy. The overall solubility parameter δ_t can be expressed by:

$$\delta_t^2 = \delta_d^2 + \delta_p^2 + \delta_h^2 \quad (2)$$

Table 1. The solubility of films with 1wt% PAG before and after (the value in the bracket) exposure in different solvents (1: insoluble within 3 minutes; 2: soluble between 5s- 3 min; 3: soluble within 5s). For solvents where there is no difference in solubility before and after exposure only one number is reported.

Solvent	MAA		tDMA		IBA		2MBA	
	Hf	Zr	Hf	Zr	Hf	Zr	Hf	Zr
Water	1	1	1	1	1	1	1	1
Methanol	3	3	3	3	1	1	1	1
Acetonitrile	3	3	3(1)	3	1	1	1	1
Isopropyl alcohol	1	2(1)	3(1)	3(2)	1	3	3	3
DMF	3	3	3	3	1	3	3	3
Acetone	3	3	3	3	3	3	3	3
Butanone	3	3	3	3	3	3	3	3
Ethyl acetate	3	3	3	3	3	3	3	3
4M2P	3(2)	2(1)	2(1)	3(2)	1	3	3	3
PGMEA	3(2)	3(2)	3	3	3	3	3	3
Methyl isobutyl	3(2)	3(2)	3	3	3	3	3	3
n-butyl acetate	3	3(2)	3	3	3	3	3	3
Methylenechloride	3	3	3	3	3	3	3	3
Chloroform	3	3	3	3	3	3	3	3
Chlorobenzene	1	3(1)	3	3	3	3	3	3
Toluene	1	1	3(2)	3(2)	1	3	3	3
Decalin	1	1	1	1	1	1	3	3

The Hansen solubility parameter can be visualized as independent points (δ_d, δ_p, δ_h) in a three-dimensional coordinates plot. Nanoparticles are well dispersed into solvents with similar solubility parameters.[23] The three dimensional Hansen solubility plot for HfIBA in different solvents before exposure to DUV is presented in Figure 2-a as a representative example. Different colours were used for clarity: red refers to films that are insoluble within 3 minutes while green represents films that are soluble within 5 seconds. Solvents represented by the green points define a sphere within which the solubility is good.[22, 24] The solubility sphere is more apparent in the 2D, triangular Teas graph, as shown in Figure 2-b, which uses a set of fractional parameters derived from the Hansen values to represent contributions from dispersion, polar and hydrogen bonding interactions.[14, 25, 26] The radius, denoted as the interaction radius, and the center of the solubility sphere obtained by fitting all data using a previously reported approach are 12.2 $MPa^{1/2}$ and (δ_d=20.0, δ_p= 7.7, δ_h= 10.3).[27] Detailed information about the solubility parameters of the solvents used and the hybrid nanoparticles is given in Table S2. Regardless of the core, the solubility parameters are similar for nanoparticles surface-modified with 2MBA and tDMA. However, there are distinct differences between the solubility parameters of Zr- and Hf-based nanoparticles modified with MAA. In general, the dispersion contribution is highest for 2MBA-modified particles while the polar contribution is the lowest.

The solubility characteristics of films containing 1wt% PAG before and after exposure are listed in Table 1. Both (Hf, Zr)MAA and (Hf, Zr)tDMA are more difficult to be dissolved in some organic solvents after exposure, while no apparent solubility change was observed for the (Hf, Zr)2MBA and (Hf, Zr)IBA films. Even with a PAG content of 5 wt%, the solubility of (Hf, Zr)2MBA and (Hf, Zr)IBA films were unchanged compared with HfMAA and ZrMAA, which experience a larger solubility change before and after exposure. The results are consistent with earlier findings in our group showed that the MAA based films had better EUV patterning performance with higher sensitivity and smaller line edge roughness (LER).[4]

Considering the solubility of nanoparticles in specific solvents, it is interesting to note that all films were insoluble in water, while only (Hf, Zr) 2MBA can be dissolved in decalin. All films can be dissolved in acetone, methyl ethyl ketone, ethyl acetate, chloroform, and methylenechloride, before or after DUV exposure. In addition to the above mentioned solvents, all films were soluble in PGMEA, methyl isobutyl ketone, and n-butyl acetate before exposure. Both (Hf, Zr)IBA and (Hf, Zr)2MBA are insoluble in methanol and acetonitrile, two solvents that have high contributions from polar molecular interactions. In contrast, (Hf, Zr)MAA and (Hf, Zr)tDMA are soluble in the same solvents. In view of the solubility changes before and after exposure, 4- methanol-2-pentanol was chosen as the development solvent since all (Hf, Zr)MAA and (Hf, Zr)tDMA films experience low solubility after DUV exposure.

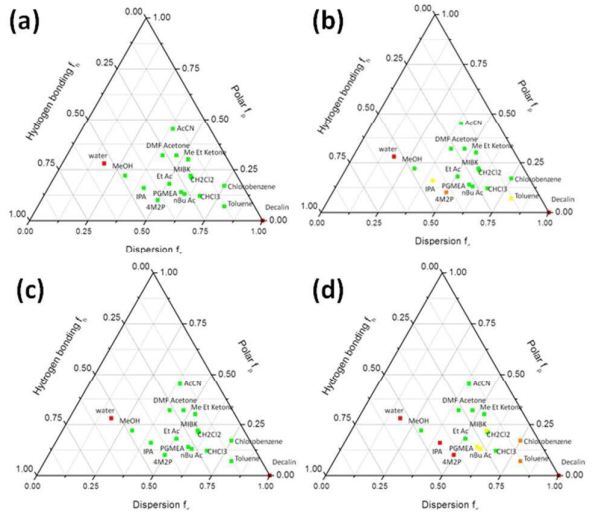

Figure 3. Teas graph of the solubility for ZrtDMA films with 1 wt% PAG (a) before exposure and (b) after exposure; 5 wt% PAG: (c) before exposure and (d) after exposure. The color scheme is similar to that in Figure 2. In addition, "yellow" refers to films soluble between 5 s and 1 min and "orange" refers to films soluble between 1 min and 3 min.

The influence of PAG content (1 wt% and 5 wt%) on the solubility change before and after exposure is shown in Figure 3. The solubility of the films with different PAG contents is the same before exposure. However, after exposure the time to dissolve in 4-methanol-2-pentanol, isopropyl alcohol and toluene is prolonged for the film with 1 wt% PAG. The solubility change is even more apparent in the film with 5 wt% PAG. The latter is less soluble in 4-methanol-2-pentanol and isopropyl alcohol, which can dissolve films containing 1 wt% PAG. Solubility of the film in other solvents, such as PGMEA, methyl isobutyl ketone, n-butyl acetate, toluene and chlorobenzene, was also weakened. (Hf, Zr)2MBA and (Hf, Zr)IBA films underwent a different trend with PAG addition, where an increase in PAG concentration did not lead to any detectable solubility changes.

One of the major developments in this paper is elucidating the relationship between the surface chemistry of hybrid nanoparticles and their solubility and stability. To start, the nanoparticles functionalized with different carboxylic ligands have a particle size of 2-3 nm with a very narrow size distribution and appear stable towards aggregation. This indicates that the electrostatic/steric stabilization is effective enough for all ligands to prevent aggregation.[28, 29] The narrow particle size distribution is also important because the presence of large particles together with smaller ones can unbalance the interparticle potential in solvents, leading to agglomeration or even precipitation.[30] Small nanoparticles with narrow size distributions are also beneficial for high-resolution photo-patterning.

That the surface ligands determine the solubility of the nanoparticles confirms that the surface functional groups dominate and can tune the solubility properties of the nanoparticles. Arita et al. have suggested that the surface ligands may weaken or even shield the interaction between solvent molecules and the metal oxide core.[23]

The presence of double bonds in the ligands increased the polar contribution of the tDMA and MAA based particles. Nanoparticles surface-functionalized with IBA and 2MBA have larger non-polar atomic dispersion than those based on tDMA and MAA. This may be the reason why (Hf,Zr)2MBA can be dissolved in decalin, a non-polar solvent.

The solubility/dispersion of hybrid nanoparticles in water should be distinguished from the dispersion in other organic solvents. The dispersion of TiO_2 surface modified with carboxylic acid is reported to be pH dependent.[31, 32] The carboxylic acid surface ligands can dissociate within the specific pH range increasing the electrostatic repulsion and promoting the dispersion of the nanoparticles. In the current case, all nanoparticles systems show poor dispersion in water, which may be because the interaction between surface carboxylic acid ligands and water molecules is not strong enough under the current pH conditions.[32]

Solvent molecules typically can bind to the surface ligands of nanoparticles by weak physisorption or donor/acceptor interactions.[20] Therefore, the influence of hydrogen-bonding ability in different solvents should also be considered, since the carboxylic acid ligands are considered strong hydrogen bond donors.[32] According to measurements by Taft and coworkers,[34, 35] nanoparticles functionalized with carboxylic acid should be well dispersed into solvents with hydrogen bond acceptor capabilities. The good solubility in acetone, chloroform, and methylene chloride are in good agreement with the work reported previously.

An important observation is that the nanoparticles functionalized with unsaturated MAA and tDMA ligands show an apparent solubility change after exposure to DUV. In contrast, the solubility change for nanoparticles functionalized with saturated 2MBA and IBA is less. This is important as we optimize the development conditions for the photoresists.

The patterning formation is complicated and affected by several factors.[12] We proposed earlier that the solubility change of the nanoparticles before and after UV exposure is based on ligand exchange with those released from the photoactive compound. For example, we hypothesized that the sulphonic acid produced from PAG after UV exposure has stronger binding energy to the metal oxide core and replaces MAA as a ligand.[6, 36] The ligand exchange can alter the surface charge of the nanoparticles and thus lead to the variation of electrostatic double layer width leading to a solubility change.

More recently we reported that the particle size of Hf nanoparticles functionalized with benzoic acid (BA), MMA and DMA increases after UV irradiation and that the photosensitivity increased in that order.[12] Since solubility/dispersion of the nanoparticles can be correlated to their size the results reported here are consistent our previous work. Recall that the largest change in solubility was observed for particles decorated with ligands containing double bonds (e.g. MMA and DMA).

Conclusions

To conclude, the solubility characteristics of hybrid nanoparticles composed of a metal oxide core (ZrO_2 and HfO_2) and decorated with different carboxylic acids were investigated in detail. All nanoparticles show a hydrodynamic diameter of 2-3 nm and a very narrow size distribution in organic solvents both of which contribute to their high stability and patterning resolution. Since the surface ligands determine the solubility of the nanoparticles their solubility can be optimized accordingly. The Hansen solubility parameters for nanoparticles functionalized with IBA and 2MBA have the highest contributions from the dispersion interaction than those with tDMA and MAA, which show more polar character. The nanoparticles functionalized with unsaturated surface ligands showed more apparent solubility changes after exposed to DUV than those with saturated. The solubility differences after exposure are more pronounced for films containing a higher amount of photoacid generator. The results reported here are consistent with our previous work, where Hf oxide nanoparticles decorated with DMA and MMA were more photosensitive compared to BA containing analogues leading to corresponding increases in their particle size upon UV exposure. That the surface ligands determine the solubility of the nanoparticles confirms that the surface functional groups dominate and can tune the solubility properties of the nanoparticles. The detailed study reported here provides a rational framework to select and optimize ligands and solvents for processing and development of next generation photoresists.

Acknowledgements

The authors gratefully acknowledge funding support from SEMATECH and facilities support from Lawrence Berkeley National Laboratory (LBNL), Cornell Nanoscale Science and Technology (CNF), the Cornell Center for Materials Research (CCMR) and the KAUST-Cornell Center of Energy and Sustainability (KAUST-CU).

Notes and references

1. T. Itani and T. Kozawa, *Jpn. J. Appl. Phys.*, 2013, 52, 0002.
2. B. Wu and A. Kumar, *J. Vac. Sci. Technol., B*, 2007, 25, 1743.
3. C. Wagner and N. Harned, *Nat. Photon.*, 2010, 4, 24.
4. M. Trikeriotis, M. Krysak, Y. S. Chung, C. Ouyang, B. Cardineau, R. Brainard, C. K. Ober, E. P. Giannelis and K. Cho, *J. Photopolym. Sci. Technol.*, 2012, 25, 583.
5. W. J. Bae, M. Trikeriotis, J. Sha, E. L. Schwartz, R. Rodriguez, P. Zimmerman, E. P. Giannelis and C. K. Ober, *J. Mater. Chem.*, 2010, 20, 5186.
6. M. Krysak, M. Trikeriotis, C. Ouyang, S. Chakrabarty, E. P. Giannelis and C. K. Ober, *J. Photopolym. Sci. Technol.*, 2013, 26, 659.
7. R. Ganesan, J. Dumond, M. S. M. Saifullah, S. H. Lim, H. Hussain and H. Y. Low, *ACS Nano*, 2012, 6, 1494.
8. S. H. Lim, M. S. M. Saifullah, H. Hussain, W. W. Loh and H. Y. Low, *Nanotechnology*, 2010, 21, 285303.
9. S.-H. Wang, Y.-S. Sun, A. S.-T. Chiang, H.-F. Hung, M.-C. Chen and K. Wood, *J. Phys. Chem. C*, 2011, 115, 11941.
10. J. Stowers and D. A. Keszler, *Microelectron. Eng.*, 2009, 86, 730.
11. M. Trikeriotis, M. Krysak, Y. S. Chung, C. Ouyang, B. Cardineau, R. Brainard, C. K. Ober, E. P. Giannelis and K. Cho, *SPIE Advanced Lithography,* 2012, 83220U.
12. L. Li, S. Chakrabarty, K. Spyrou, C. K. Ober and E. P. Giannelis, *Chem. Mater.*, 2015, 27, 5027.
13. A. J. Guenthner, K. R. Lamison, L. M. Lubin, T. S. Haddad and J. M. Mabry, *Ind. Eng. Chem. Res.*, 2012, 51, 12282.
14. B. A. Miller-Chou and J. L. Koenig, *Prog. Polym. Sci.*, 2003, 28, 1223.
15. S. Doeuff, M. Henry, C. Sanchez and J. Livage, *J. Non-Cryst. Solids*, 1987, 89, 206.
16. S. M. Khaled, R. Sui, P. A. Charpentier and A. S. Rizkalla, *Langmuir*, 2007, 23, 3988.
17. R. Sui, A. S. Rizkalla and P. A. Charpentier, *J. Phys. Chem. B*, 2006, 110, 16212.
18. A. Bakalova, H. Varbanov, R. Buyukliev, G. Momekov and D. Ivanov, *J. Therm. Anal. Calorim.*, 2009, 95, 241.
19. M. Hatzakis, K. J. Stewart, J. M. Shaw and S. A. Rishton, *J. Electrochem. Soc.*, 1991, 138, 1076.
20. J. U. Wieneke, B. Kommob, O. Gaer, I. Prykhodko and M. Ulbricht, *Ind. Eng. Chem. Res.*, 2011, 51, 327.
21. J. H. Hildebrand and R. L. Scott, *The solubility of nonelectrolytes*, Reinhold, New York, 1950.
22. C. M. Hansen, *J. Paint Technol.*, 1967, 39, 505.
23. T. Arita, Y. Ueda, K. Minami, T. Naka and T. Adschiri, *Ind. Eng. Chem. Res.*, 2009, 49, 1947.
24. C. M. Hansen, *Ind. Eng. Chem. Prod. Res. Dev.*, 1969, 8, 2.
25. J. P. Teas, *J. Paint Technol.*, 1968, 40, 19.
26. J. D. Crowley, G. S. Teague Jr and J. W. Lowe Jr, *J. Paint Technol.*, 1966, 38, 269.
27. F. Gharagheizi, *J. Appl. Polym. Sci.*, 2007, 103, 31.
28. R. Bywalez, H. Karacuban, H. Nienhaus, C. Schulz and H. Wiggers, *Nanoscale Res. Lett.*, 2012, 7, 1.
29. T. Akesson, C. Woodward and B. Jonsson, *J. Chem. Phys.*, 1989, 91, 2461.
30. T. Arita, J. Yoo, Y. Ueda and T. Adschiri, *Nanoscale*, 2010, 2, 689.
31. T. Arita, K.-i. Moriya, K. Minami, T. Naka and T. Adschiri, *Chem. Lett.*, 2010, 39, 961.
32. T. Arita, K. Moriya, T. Yoshimura, K. Minami, T. Naka and T. Adschiri, *Ind. Eng. Chem. Res.*, 2010, 49, 9815.
33. G. K. Rowe and S. E. Creager, *J. Phys. Chem.*, 1994, 98, 5500.
34. R. W. Taft and M. J. Kamlet, *J. Am. Chem. Soc.*, 1976, 98, 2886.
35. M. J. Kamlet and R. W. Taft, *J. Am. Chem. Soc.*, 1976, 98, 377.
36. B. Cardineau, M. Krysak, M. Trikeriotis, E. Giannelis, C. K. Ober, K. Cho and R. Brainard, 2012.